Nanoscale

PAPER

View Article Online
View Journal | View Issue

Cite this: *Nanoscale*, 2018, **10**, 9133

A gold-nanoparticle stoppered [2]rotaxane†

Anne Ulfkjær,[a] Frederik W. Nielsen,[a] Hana Al-Kerdi,[a] Tamara Ruß,[a] Zaki K. Nielsen,[a] Jens Ulstrup,[b] Lanlan Sun,[c] Kasper Moth-Poulsen,*[c] Jingdong Zhang*[b] and Michael Pittelkow*[a]

The construction of molecular machines has captured the imagination of scientists for decades. Despite significant progress in the synthesis and studies of the properties of small-molecule components (smaller than 2–5 kilo Dalton), challenges regarding the incorporation of molecular components into real devices are still eminent. Nano-sized molecular machines operate the complex biological machinery of life, and the idea of mimicking the amazing functions using artificial nano-structures is intriguing. Both in small-molecule molecular machine components and in many naturally occurring molecular machines, mechanically interlocked molecules and structures are key functional components. In this work, we describe our initial efforts to interface mechanically-interlocked molecules and gold-nanoparticles (AuNPs); the molecular wire connecting the AuNPs is covered in an insulating rotaxane-layer, thus mimicking the macroscopic design of a copper wire. Taking advantage of recent progress in the preparation of supramolecular complexes of the cucurbit[7]uril (CB[7]) macrocycle, we have prepared a bis-thiol functionalised pseudo-rotaxane that enables us to prepare a AuNP-stoppered [2]rotaxane in water. The pseudo-rotaxane is held together extremely tightly ($K_a > 10^{13}$ M^{-1}), K_a being the association constant. We have studied the solution and gas phase guest–host chemistry using NMR spectroscopy, mass spectroscopy, and electrochemistry. The bis-thiol functionalised pseudo-rotaxane holds further a ferrocene unit in the centre of the rotaxane; this ferrocene unit enables us to address the system in detail with and without CB[7] and AuNPs using electrochemical methods.

Received 26th February 2018,
Accepted 5th April 2018

DOI: 10.1039/c8nr01622d

rsc.li/nanoscale

Introduction

Mechanically-interlocked molecules are of significant importance for the development of molecular machines at the molecular level.[1–3] At the small-molecule level, the work of Sauvage, Sanders, Leigh, Stoddart, and others since the 1970s has enabled the preparation of complex structures ranging from rotaxanes through catenanes to molecular knots.[1–4] Exploitation of the unique properties of these structures has enabled complex operations such as unidirectional motion and on–off-switches for electronic components.[1–5] The importance of naturally occurring systems that feature mechanically-interlocked structures is being realised in recent years. The discoveries of knotted DNA strands and lasso peptides are recent examples.[6,7]

Nano-engineering offers a unique opportunity for bridging the gap between the many-nanometre size-regimes of the biological world and the Ångström world of small molecules. Artificial molecular machine immobilized surfaces (AMMISs), where for example (pseudo)rotaxanes have been attached onto gold surfaces, are examples.[8–10] The preparation of metallic nanoparticles (NPs) with well controlled size, multifarious functional groups and manipulation of their properties have revolutionized nanoscience and nanotechnology. The most studied metal NPs are gold nanoparticles (AuNPs), now a core nanoscale physical entity with applications ranging from molecular electronics and molecular biology to the self-assembly of dynamic combinatorial libraries that lead to sophisticated molecular recognition phenomena.[11–13] In the context of molecular electronics, AuNPs can be regarded as potential ultra-small electrodes, and the unique optical and electronic properties of AuNPs have been explored for the development of biosensors and biomedicine.[14–23]

Connecting AuNPs with conducting molecular wires or electrochemically active molecular components is an intriguing perspective. If AuNPs are connected *via* a mechanically interlocked structure, for example a pseudo-rotaxane, one can envi-

[a]*Department of Chemistry, University of Copenhagen, Universitetsparken 5, DK-2100 Copenhagen, Denmark. E-mail: pittel@chem.ku.dk*
[b]*Department of Chemistry, Technical University of Denmark, Kemitorvet, Building 207, DK-2800 Kongens Lyngby, Denmark. E-mail: jz@kemi.dtu.dk*
[c]*Department of Chemistry and Chemical Engineering, Chalmers University of Technology, Kemivägen 4, SE-41296 Gothenburg, Sweden. E-mail: kasper.moth-poulsen@chalmers.se*

†Electronic supplementary information (ESI) available: Experimental procedures, spectral characterisation data, details of the binding studies, and a description of the electrochemical measurements. See DOI: 10.1039/c8nr01622d

sage a molecular wire connecting the AuNPs covered in an insulating layer, thus mimicking the macroscopic design of a copper wire. Success in this area would potentially enable constructing very small electronic components (Fig. 1).

Recent developments in the area of supramolecular chemistry of the macrocycles cucurbit[*n*]urils (CB[*n*]) in aqueous solution have been utilized to enable the formation of very stable pseudo-rotaxanes; a bis-dialkylammonium ferrocene compound with an association constant to CB[7] of 3×10^{15} M^{-1} in water was discovered in 2007, and in 2014, the first host–guest pair with a dissociation constant as small as 10^{-18} M was reported for CB[7].[24] Such high binding affinities mean that the complexes are essentially completely intact, even at extremely low concentrations, which makes these pseudo-rotaxanes compatible with the concentrations where AuNPs are prepared.

We report here the preparation of a [2]rotaxane with AuNPs functioning as stoppers and an electroactive ferrocene core structure surrounded by a CB[7] moiety. To achieve this, the preparation of a pseudo-rotaxane with two thiols pointing out of CB[7] is essential. Specifically, we describe the synthesis and investigation of two inclusion complexes based on the CB[7] host and a novel ferrocene based bis-ammonium cationic guest molecule functionalised with thiols (Chart 1). The complexes have been systematically characterised by liquid chromatography-mass spectrometry (LC-MS), 1D and 2D nuclear magnetic resonance (NMR) spectroscopy as well as electrochemical investigations. The electrochemical data are of particular interest as they disclose detailed insight into the dynamics of the pseudo-rotaxane structure. ^{1}H NMR competition experiments reveal extremely strong binding affinities of the complexes ($K_a \sim 10^{13}$ M^{-1}) and the possibility of reversibly removing the functionalised guest upon treatment with a competitive guest molecule. Finally, we confirm the formation of a simple [2]rotaxane structure by transmission electron microscopy (TEM).

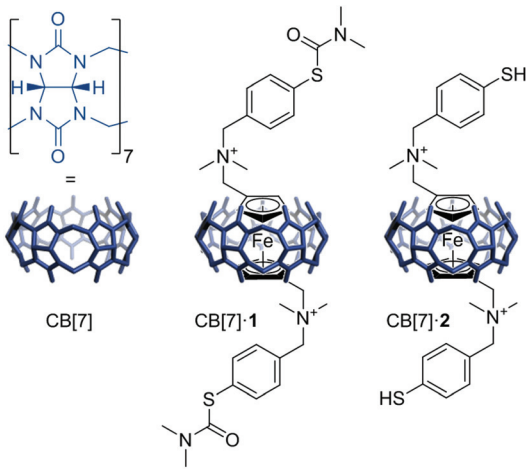

Chart 1 Structures of the CB[7] host and the inclusion complexes between CB[7] and the ferrocene guests **1** and **2** reported in this work.

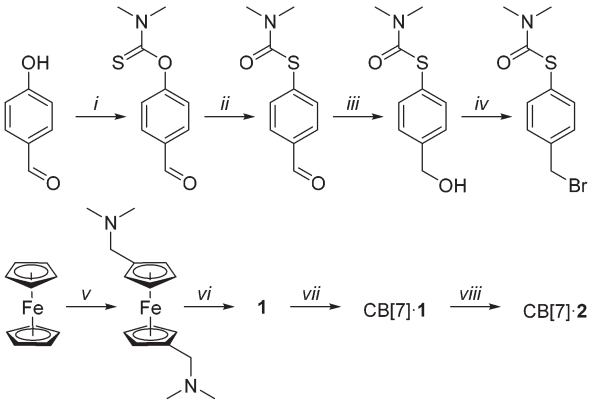

Scheme 1 Synthesis of **1**, CB[7]·**1**, and CB[7]·**2**. Reagents and conditions: (i) DABCO, $(CH_3)_2NCSCl$, NMP, 50 °C, 17 h, 95%; (ii) Ph_2O, 270 °C, 45 min, 79%; (iii) $NaBH_4$, MeOH, 0–25 °C, 21 h, 97%; (iv) PBr_3, CH_2Cl_2, 0 °C – reflux, 21 h, 78%; (v) (a) *n*-BuLi, TMEDA, hexane, 25 °C, 22 h, (b) $[(CH_2{=}N(CH_3)_2)I]$, 25 °C – reflux, 22 h, 69%; (vi) benzyl bromide, MeOH, reflux, 10 min, 78%; (vii) CB[7], KCl, H_2O, 25 °C, spontaneously, quant.; (viii) NaOH, KCl, H_2O, 25 °C, 22 h, 82%.

Results and discussion

Synthesis of the inclusion complexes

Guest **1** was synthesised using a convergent synthesis strategy (Scheme 1). The phenyl moiety was introduced from 4-hydroxybenzaldehyde and the *O*-thiocarbamate formed through a reaction with *N*,*N*-dimethylthiocarbamoyl chloride. A thermally induced Newman–Kwart rearrangement[25] converted the *O*-thiocarbamate into the corresponding *S*-thiocarbamate. Selective reduction using $NaBH_4$ transformed the aldehyde into the alcohol and was followed by a reaction with PBr_3 to generate the benzyl bromide intermediate.

The dialkylation of the ferrocene moiety was conducted through the lithiation of ferrocene with *n*-BuLi followed by an *in situ* reaction with Eschenmoser's salt.[26] Adding the benzyl bromide intermediate to the alkylated ferrocene intermediate formed the quaternary ammonium cations *via* a Menshutkin reaction yielding the bromide salt of guest **1**.

The inclusion complex CB[7]·**1** was formed spontaneously when mixing equimolar amounts of guest **1** together with the CB[7] host, which was synthesised according to a reported

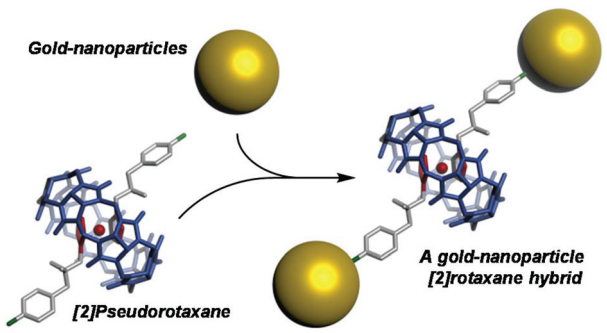

Fig. 1 Schematic representation of the formation of a gold-nanoparticle [2]rotaxane hybrid from a [2]pseudorotaxane and gold-nanoparticles.

procedure.[27] Subsequent basic hydrolysis of the *S*-thiocarbamates in CB[7]·**1** gave the CB[7]·**2** complex. All compounds were characterised by ^{1}H and ^{13}C NMR spectroscopy, high-resolution ESI mass spectrometry, and elemental analysis thus confirming their identities (see the ESI†).

Characterisation by NMR spectroscopy

^{1}H NMR spectroscopy provides an initial assessment of the binding interactions between the cationic ferrocene guests and the CB[7] host. The ^{1}H NMR spectra of **1**, CB[7], and CB[7]·**1** are shown in Fig. 2a. The complex formation induces changes in the chemical shift values of both CB[7] and **1**. The presence of CB[7] leads to a pronounced upfield shift of the proton resonances in the cyclopentadienyl (Cp) ring with $\Delta\delta$ values of 0.75 ppm for H_G and 0.83 ppm for H_H. In contrast, the signals corresponding to the protons on the substituted phenyl ring (H_A, H_B, and H_C) experience only a small downfield shift. The reverse trend in the two moieties of **1** indicates entirely different environments for the ferrocene and phenyl group, showing how the ferrocene residue is positioned inside the cavity of CB[7] upon complexation, while the phenyl moiety remains outside. The methylene and *N*-methyl protons (H_D and H_E) are less shielded, moving upfield with $\Delta\delta$ values of 0.11 and 0.04 ppm, respectively, which indicates that they are closer to the cavity than the protons H_A–H_C. Finally, the methylene protons (H_F) that bridge the ferrocene unit to the positively charged nitrogen are shifted upfield ($\Delta\delta$ 0.64 ppm) along with the ferrocene protons, providing clear evidence that they are all fully included by CB[7]. Similar spectral changes were observed for CB[7]·**2** (Fig. 2a, bottom).

A 2D ROESY experiment on the complex CB[7]·**1** further supports that the ferrocene moiety in **1** is located inside the cavity of CB[7]. The ^{1}H–^{1}H ROESY spectrum displays strong electronic couplings shown as NOE cross peaks from H_G and H_H on ferrocene to the CB[7] proton H_J and none to H_I (Fig. 2b). This suggests that the ferrocene moiety and the cavity of CB[7] are in close proximity through space thus forming the inclusion complex CB[7]·**1**.

Diffusion ordered ^{1}H NMR spectroscopy (DOSY) on CB[7]·**1** was consistent with the presence of a single species in solution with a diffusion coefficient (D) of 3.8×10^{-6} cm^2 s^{-1} (Fig. 2c). This result points towards a high association constant between CB[7] and **1**, as the DOSY peaks for these two species converge, showing how the host and guest diffuse together as a single molecular entity. Adding excess CB[7] to this sample resulted in two sets of separated signals with different diffusion coefficients; one corresponding to CB[7]·**1** with a lower D value and one with a higher value corresponding to the smaller CB[7] species ($D_{CB[7]} = 4.2 \times 10^{-6}$ cm^2 s^{-1}; Fig. 2d).

The NMR spectroscopic data thus provide strong evidence for the location of the CB[7] host around the ferrocene residue in the CB[7]·**1** and CB[7]·**2** complexes.

Association constants

In the preliminary ^{1}H NMR experiments, it was observed that the CB[7]·**1** and CB[7]·**2** complexes formed quantitatively with

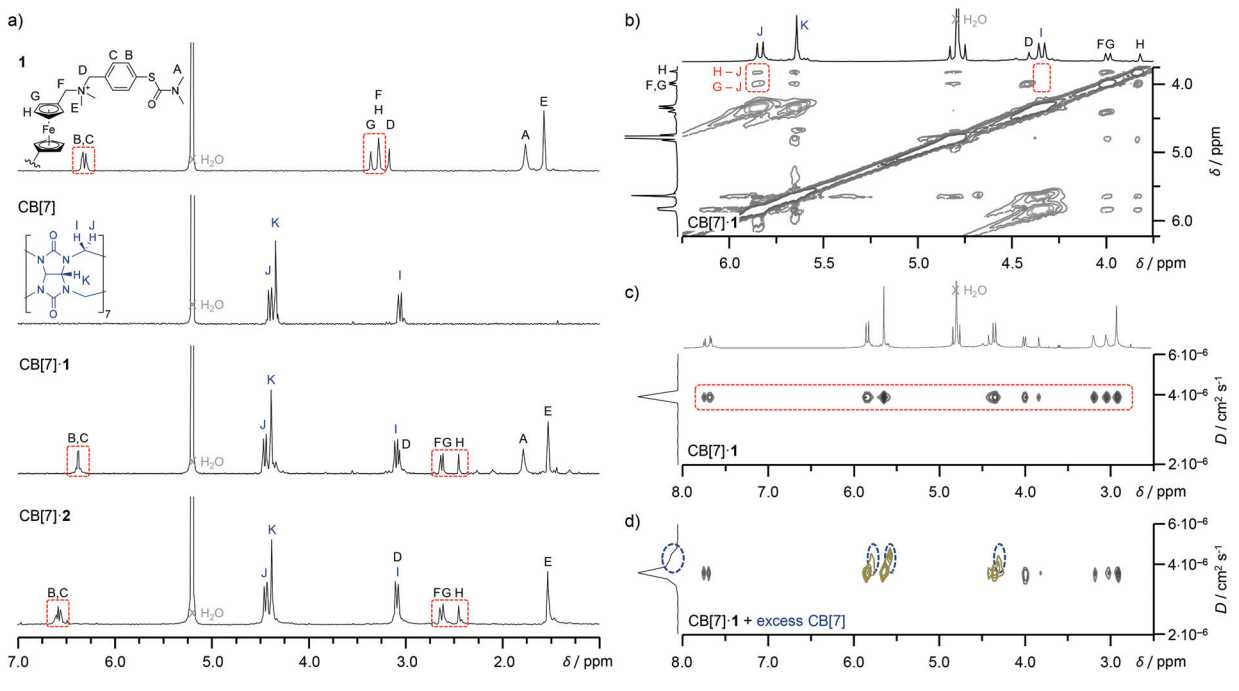

Fig. 2 NMR analysis of the compounds synthesised showing (a) stacked ^{1}H NMR spectra (100 mm KCl in 4 M DCl$_{(aq)}$, 500 MHz, 25 °C) of **1**, CB[7], CB[7]·**1**, and CB[7]·**2**; (b) partial ^{1}H–^{1}H ROESY spectrum (500 MHz, 100 mM KCl in D_2O, 25 °C) of CB[7]·**1**; (c) ^{1}H DOSY spectrum (500 MHz, 100 mM KCl in D_2O, 25 °C) of CB[7]·**1** ($D_{CB[7]\cdot 1} = 3.8 \times 10^{-6}$ cm^2 s^{-1}); and (d) ^{1}H DOSY spectrum (500 MHz, 100 mM KCl in D_2O, 25 °C) of CB[7]·**1** added excess CB[7] where the blue signals arise from excess CB[7] ($D_{CB[7]} = 4.2 \times 10^{-6}$ cm^2 s^{-1}). Assignment of the signals is based on the labelling shown on the structures in the figure.

only millimolar concentrations of the host and guest, suggesting that the association constant (K_a) is high. Furthermore, the ^{1}H NMR spectra of CB[7]·**1** when an excess amount of guest was present showed how the signals of the free and bound guest were simultaneously observed, revealing that the rate of exchange between these species is slow on the NMR time scale. These findings were anticipated since similar observations in other CB[7]·ferrocene complexes have been reported, where the high stability was proven through extremely high binding affinities (10^9–10^{15} M^{-1}).[24,28,29]

The large association constant precludes determination of K_a for the complex formation between CB[7] and **1** directly by NMR spectroscopy as they exceed the experimentally accessible range ($10 < K_a < 10^4$ M^{-1}).[30] A competition ^{1}H NMR spectroscopic experiment was instead carried out, where guest **1** together with a reference guest (1,1′-bis(*N*,*N*,*N*-trimethylammoniomethyl)ferrocene, **3**)[29] was allowed to compete for a limited amount of the host, CB[7]. Using this procedure an association constant of 1.1×10^{13} M^{-1} for the complexation between CB[7] and **1** in 100 mM KCl in D_2O was determined (ESI, section S3†).

The K_a value obtained for CB[7]·**1** is one of the highest binding affinities reported for a monovalent synthetic host–guest complex and is comparable in strength to the values in supramolecular chemistry and the biologically widely used avidin–D-biotin pair.[31] This result reflects the unique binding properties of CB[7] towards guest **1** and shows that ultra-high binding affinities competitive with biological receptor molecules can be achieved for purely synthetic systems.

Our attempts to obtain single crystals of CB[7]·**1** and CB[7]·**2** suitable for X-ray diffraction analysis failed, verifying the difficulties often encountered when trying to crystallize CB[7]·guest complexes.[32] However, the crystal structure of the complex CB[7]·**3** previously obtained can be used as a model to describe the core interactions in CB[7]·**1**.[24] Here, the X-ray structure shows how the ferrocene residue is included by the CB[7] cavity filling approximately 55% of the host cavity volume, which is the optimum cavity-filling fraction as proposed by Mecozzi and Rebek.[33] The near perfect size/shape complementarity between the rigid CB[7] cavity and the ferrocene moiety is another factor leading to the formation of the highly stable CB[7]·**1** complex.

Characterisation by LC/MS

Mass spectrometry is now an important tool for characterisation of stable inclusion complexes in the gas phase. This technique can provide unique insight into the formation of the complexes and their stoichiometries, and thereby serves as a supplement to condensed phase studies.[34] A combination of high performance liquid chromatography (HPLC) and high-resolution electrospray ionization time-of-flight mass spectrometry (HR-ESI-TOF-MS) was employed for the studies of the inclusion complexes CB[7]·**1** and CB[7]·**2**. Fig. 3a shows the HPLC chromatograms of **1**, CB[7]·**1**, and CB[7]·**2** monitored at 255 nm, where CB[7] alone is not UV active. Each chromatogram presents one sharp, well-defined peak with a retention

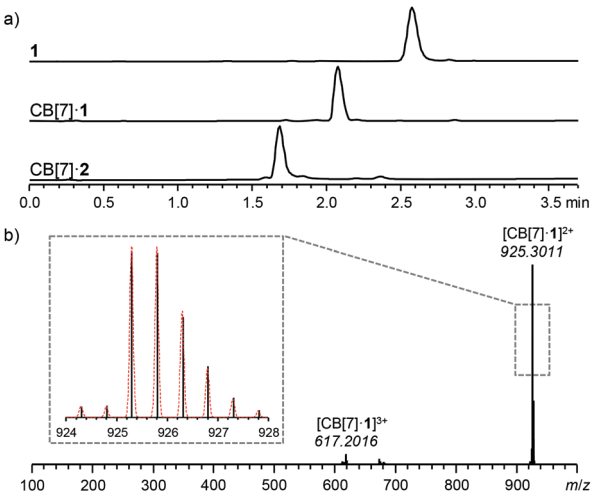

Fig. 3 LC/MS analysis of the target compounds showing (a) stacked HPLC chromatograms (255 nm) of **1** (top), CB[7]·**1** (middle), and CB[7]·**2** (bottom), and (b) HR-ESI-TOF-MS spectrum of CB[7]·**1**. The inset shows a zoom of the isotopic distribution of the main peak where the calculated distribution is shown as red dotted lines while the black lines are the measured spectrum.

time of 2.6, 2.1, and 1.7 minutes as the analyte changes from **1** through CB[7]·**1** to CB[7]·**2**. The distinct peaks indicate that the inclusion complexes persist throughout the column and do not degrade or dissociate.

The corresponding mass spectrum of CB[7]·**1** is shown in Fig. 3b where the main peak in the spectrum, at an *m*/*z* ratio of 925.3011, is a doubly charged peak shown in the inset together with the calculated isotopic distribution. This peak is consistent with one doubly charged bis-ammonium cation **1** enclosed by the neutral CB[7] host, $[CB[7]\cdot\mathbf{1}]^{2+}$, verifying the 1 : 1 inclusion complex. A second minor peak, at an *m*/*z* ratio of 617.2016, which matches the triply charged inclusion complex $[CB[7]\cdot\mathbf{1}]^{3+}$ is also present. We suggest that the third positive charge is acquired through the oxidation of the ferrocene unit in the compound thereby reflecting the relative ease of oxidation of the ferrocene/ferrocenium unit in the compound (see the Electrochemical characterisation section below), as seen previously for related compounds.[35]

Non-covalent complexes tend to dissociate during LC/MS runs. This can happen both when the complex passes through the polar, aqueous mobile phase in the column of the HPLC or in the spray process in the mass spectrometer, where the association energy of the complex becomes lower than the dissociation energy. However, here the CB[7]·**1** complex persisted throughout the column as well as in the transition from the solution to gas phase and was detected without any fragmentation, testifying to a high association energy of CB[7]·**1**. Similar results were obtained for CB[7]·**2** (ESI, Fig. S36†).

Electrochemical characterisation

Ferrocene derivatives are electrochemically active, exhibiting fast and reversible one-electron oxidation.[36] This offers an

additional approach to examine the CB[7]·guest host–guest interactions. We investigated the electrochemical properties of the ferrocene derivatives in the absence and presence of the CB[7] host in aqueous solution using cyclic voltammetry (CV). The cyclic voltammogram of **1** shows one set of well-defined peaks corresponding to reversible one-electron transfer of the ferrocene (Fc)/ferrocenium (Fc^+) couple at a midpoint redox potential (E°) of 670 mV *vs.* the saturated calomel electrode (SCE), Fig. 4. A large anodic tail is observed at a higher potential (>900 mV *vs.* SCE) and is caused by the oxidation of bromide counter ions to the ammonium cations in **1**, to bromine (ESI, Fig. S6†).

The addition of CB[7] to **1** forms the inclusion complex CB[7]·**1** and leads to a pronounced 172 mV anodic shift of the ferrocene E° value to 842 mV *vs.* the SCE (Table 1). This observation is consistent with the encapsulation of the ferrocene moiety inside the CB[7] cavity.[24,28,37,38] An excess of 0.3 equivalents CB[7] was added to **1** to ensure complete formation of the inclusion complex. A reference experiment with CB[7] alone, in the same potential window, showed no redox activity thus confirming that the peaks observed originate solely from the inclusion complex CB[7]·**1**. A large anodic tail in the CV of CB[7]·**1** at a high potential (>1.00 V *vs.* SCE) is again caused by the oxidation of the bromide counter ions in CB[7]·**1**.

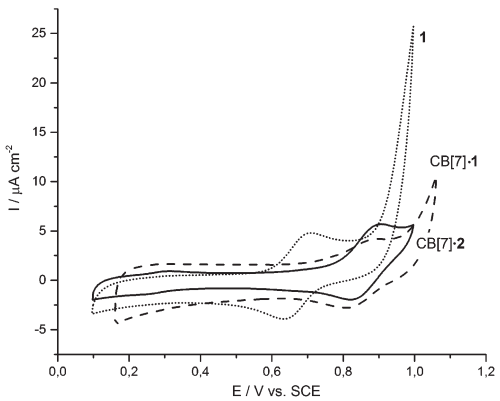

Fig. 4 Cyclic voltammograms of **1** (dotted line), CB[7]·**1** (dashed line), and CB[7]·**2** (continuous line). The samples (50 μM) are recorded using a glassy carbon electrode in aqueous KH_2PO_4 (20 mM, pH 4.6). Scan rate 50 mV s^{-1}.

Table 1 Midpoint redox potentials (E°, mV *vs.* SCE) and potential changes on the complexation of free **1** and **2** with CB[7] (ΔE°, mV *vs.* SCE). The associated changes in Gibbs free energy ($\Delta\Delta G^\circ$, kJ mol^{-1}) are also given[a]

Compound	E° [mV]	$\Delta E^{\circ b}$ [mV]	$\Delta\Delta G^{\circ c}$ [kJ mol^{-1}]
1	670	—	—
CB[7]·**1**	842	+172	−16.6
CB[7]·**2**	855	+185	−17.8

[a] Data obtained from cyclic voltammetry in aqueous 20 mM KH_2PO_4 solution (pH 4.6), 25 °C. Scan rate 50 mV s^{-1}. [b] ΔE° values calculated as E°(CB[7]·guest) − E°(**1**). [c] Obtained using $\Delta\Delta G^\circ = -\nu \cdot F \cdot \Delta E^\circ$, where ν is the number of electrons transferred in the reaction and F is the Faraday's constant.

The anodic shift in E° from **1** to CB[7]·**1** reflects the local environmental changes around the ferrocene moiety. The electroneutral reduced ferrocene moiety is considerably stabilized in the complex CB[7]·**1**. Upon reduction of the ferrocene centre, the resulting anodic shift corresponds to a free energy drop ($\Delta\Delta G^\circ$) of 16.6 kJ mol^{-1}. This decrease is caused by stabilization of the doubly charged reduced ferrocene inside the hydrophobic cavity of CB[7] relative to the triply charged oxidized form that is less favourable for CB[7] enclosure,[28,39] *i.e.* it becomes easier to reduce the oxidized form than for free **1**.

The large association constant of CB[7]·**1** is also evidenced by the electrochemical data. The CV of CB[7]·**1** shows only a single cathodic peak at 802 mV *vs.* the SCE and no signal at 630 mV *vs.* the SCE corresponding to pure **1**, indicating that the complex has not disassembled.

Similar CVs were observed for CB[7]·**2** with a midpoint redox potential of 855 mV *vs.* the SCE corresponding to an anodic shift of 185 mV *vs.* **1**. This can be ascribed to the same reasons as for **1** and CB[7]·**1**. The fact that the complexation is clearly detected at micromolar concentrations supports the high stability of these complexes. In addition, a pair of smaller peaks is observed around 278 mV *vs.* the SCE. This process is caused by the formation of carbonyl and/or quinone compounds on the carbon electrode surface, which is common for chloride containing supporting electrolytes,[40] reflecting that chloride anions are the counter ions in CB[7]·**2**.

Electrochemical kinetics of 1 and CB[7]·1. Cyclic voltammetry of solute **1**, CB[7]·**1** and CB[7]·**2** at shorter time scales, *i.e.* at faster scan rates, gives voltammetric signals that display different patterns for the three compounds (ESI, Fig. S7†). **1** follows a diffusion controlled electrochemical process for scan rates up to 0.5 V s^{-1}, with both the anodic (i_{pa}) and cathodic peak current (i_{pc}) following a scan rate (ν) dependence, $i_{pa,c} \propto \nu^x$, $x \approx 1/2$ ($R^2 = 0.996 \pm 0.001$, see ESI, Fig. S8 and S9†). This roughly applies also to CB[7]·**1**, although formally with a slightly higher $x \approx 0.6$. For **1** the peaks separate at scan rates higher than 0.5 V s^{-1}, where kinetic control and "quasi-reversible" behaviour gradually take over (see further discussion below and ESI, Fig. S11†).

The diffusion coefficients (D_o) of the electroactive species were obtained using the Randles–Sevčik equation (eqn (1)),[41]

$$i_p = 0.4463 \cdot n \cdot F \cdot A \cdot c \cdot \sqrt{\frac{n \cdot F \cdot \nu \cdot D_o}{R \cdot T}} \quad (1)$$

where n is the number of electrons in the redox process, F the Faraday's constant, A the electrode area, c the concentration of the compound, R the gas constant, and T the absolute temperature. The resulting D_o are listed in Table 2.

Among other determinants, the diffusion coefficient depends on the size (diameter) of the molecule.[42] As the CB[7]·**1** complex is bulkier than its free counterparts, the D_o(CB[7]·**1**) determined from eqn (1) is smaller (Table 2)

Table 2 Diffusion coefficients (D_o, $cm^2\ s^{-1}$) and heterogeneous electron transfer rate constants (k_s, $cm\ s^{-1}$) obtained for **1** (real), CB[7]·**1** (real) and CB[7]·**2** (apparent)[a]

Compound	pH	D_o [$cm^2\ s^{-1}$]	k_s [$cm\ s^{-1}$]
1	4.6	$(1.5 \pm 0.4) \times 10^{-6}$	$(1.4 \pm 0.1) \times 10^{-2}$
CB[7]·**1**	4.6	$(6.3 \pm 0.7) \times 10^{-7}$	$(2.8 \pm 0.2) \times 10^{-3}$
CB[7]·**2**	4.6	$(9.2 \pm 0.3) \times 10^{-5}$	$(3.9 \pm 0.1) \times 10^{-2}$
	1.4	$(10.6 \pm 0.1) \times 10^{-5}$	$(59 \pm 8) \times 10^{-2}$

[a] The data obtained from cyclic voltammetry in either KH_2PO_4 (20 mM, pH 4.6) or $HClO_4$ (20 mM, pH 1.4) at 25 °C.

reflecting the larger hydrodynamic radius of the complex, as seen previously for related systems.[38] D_0 for CB[7]·**1** is thus less than half the value for **1** ($(6.3 \pm 0.7) \times 10^{-7}$ $cm^2\ s^{-1}$ *vs.* $(1.5 \pm 0.4) \times 10^{-6}$ $cm^2\ s^{-1}$), roughly following the cross section of the molecules.

1 and CB[7]·**1** thus display consistent diffusion behaviour. The calculated D_0 for CB[7]·**2**, based on eqn (1), is, however, 16 times that for CB[7]·**1** of comparable size, and six times that for **1**. This abnormally large D_0 value for CB[7]·**2** almost certainly suggests a different electron transfer mechanism for CB[7]·**2**. While D_0 for **1** and CB[7]·**1** in Table 2 can be regarded as real diffusion coefficients, D_0 for CB[7]·**2** must therefore instead be denoted as "apparent".

Table 2 also summarizes the real and "apparent" heterogeneous electron transfer rate constants (k_s) obtained for **1**, CB[7]·**1**, and CB[7]·**2**. The ferrocene moiety in **1** was found to follow reversible behaviour at low scan rates (< 0.5 V s^{-1}), according to previous reports for similar systems.[35,38,43] Reversible processes involve fast electron transfer compared to the scan rate with only transient surface interaction between the electrode and the reagents, and a peak separation of 59 mV (for a one-electron transfer) independent of the scan rate.[42] Approximately, this behaviour was observed for **1** as evidenced by the invariance of the peak-to-peak splitting (ΔE_p = 79 ± 1 mV) as the scan rate increased up to about 0.5 V s^{-1}. The ΔE_p value is somewhat higher than the theoretical value of 59 mV which may be caused by small distortions due to solution resistance effects.[44]

When the scan rate was increased to 4 V s^{-1} the difference between the anodic and cathodic midpoint potentials of **1** was found to increase, indicating that the scan rate is now faster than the electron transfer process, and the process thus changes from reversible to quasi-reversible. The heterogeneous electron transfer rate constant k_s for **1** was determined for the quasi-reversible process using Nicholson's method (eqn (2)),[45] and calculated at given scan rates using the parameter Ψ, based on the experimental ΔE_p values, *i.e.*

$$\Psi = \frac{(D_o/D_R)^{\alpha/2} \cdot k_s \cdot \sqrt{R \cdot T}}{\sqrt{D_o \cdot \pi \cdot n \cdot F \cdot v}} \quad (2)$$

where D_0 and D_R are the diffusion coefficients of the oxidized and reduced species and α the electrochemical transfer coefficient. Taking $D_o = D_R$ and $\alpha = 0.5$, k_s for **1** was determined for all applied scan rates and found to be $(1.4 \pm 0.1) \times 10^{-2}$ $cm\ s^{-1}$ independent of the scan rate (Table 2, and the ESI†).

The complex CB[7]·**1** displays quasi-reversible behaviour at scan rates higher than 50 mV s^{-1}. The midpoint potential separation increases linearly from 79 to 325 mV as the scan rate increases from 0.05 to 4.00 V s^{-1}. The heterogeneous electron transfer rate constant was determined for CB[7]·**1** similar to **1**, giving $k_s = (2.8 \pm 0.2) \times 10^{-3}$ $cm\ s^{-1}$.

The rate constant values in Table 2 show that encapsulation of the ferrocene moiety in **1** into the complex CB[7]·**1** reduces the electrochemical rate constant by a factor of five. A similar trend was observed in related CB[7]·guest inclusion complexes.[38] The smaller rate constant can be understood by viewing the CB[7] macrocycle either as an additional physical barrier for electron tunnelling or as caused by pre-organization of the CB[7]·**1** complex towards more favourable electron transfer ("gated electron transfer")[46] adding an additional activation energy contribution. We address this difference further in the Conclusion section.

Interfacial electrochemical kinetics of CB[7]·2. The mechanistic electron transfer dynamics of CB[7]·**2** is different from that of **1** and CB[7]·**1**. The abnormal values of the "apparent" diffusion coefficient and interfacial electron transfer rate constant based on the diffusion formalism were noted. In addition the $i_{pa,c} \propto v^x$ correlation accords poorly with $x \approx 0.5$ but shows instead a $i_{pa,c} \propto v^{0.8-0.9}$ behaviour (ESI, Fig. S8 and S9†). The diffusion formalism represented by eqn (1) and (2) therefore does represent well the voltammetry of CB[7]·**2**, which accords much better with monolayer voltammetry. This is understandable if the thiolate linker group of CB[7]·**2** is adsorbed more strongly on the glassy carbon electrode surface than the thiocarbamate linkers of **1** and CB[7]·**1**. It is not *a priori* obvious that this should be so, but the obviously different voltammetric behaviour is a strong indication that this is indeed the case.

Interfacial electrochemical electron transfer kinetics of CB[7]·**2** is then more appropriately based on the Laviron analysis.[47] For the sake of completion, the Laviron analysis based standard electron transfer rate constant was calculated from the variation of the peak separation with increasing scan rate. With the reservation that the peak separations are on the small side for ideal Laviron analysis, the rate constant was found to be ~40 s^{-1} (ESI, section S5.6†) robust up to 10 V s^{-1} and 200 mV peak separation. This is a remarkably high value, testifying to highly efficient interfacial electrochemical electron transfer and strong bonding between the thiolate functionality on CB[7]·**2** and the glassy carbon electrode.

The different mechanisms and rate constant units mean, however, that the diffusion controlled and surface controlled rate constants (k_s in $cm\ s^{-1}$ *vs.* s^{-1}) cannot be compared directly. In the Conclusion section we therefore focus on the comparison of the diffusion based interfacial electrochemical rate constants of **1** and CB[7]·**1** with details given in ESI, sections S5.5–S5.7.†

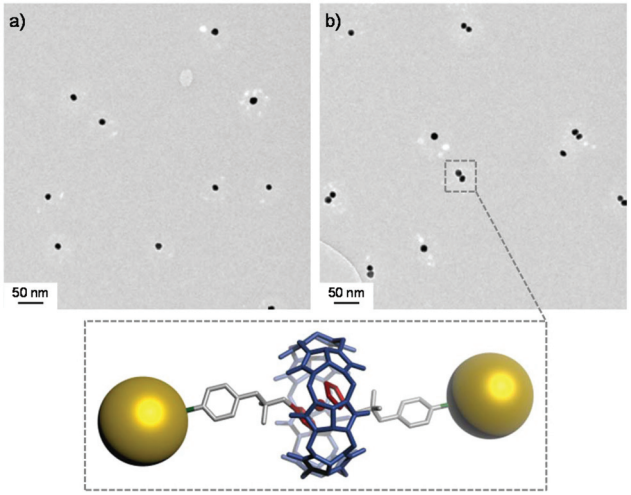

Fig. 5 TEM images of the gold nanoparticle capped [2]rotaxane showing (a) the reference AuNP (12 nm diameter, no CB[7]·**1** added) and (b) after the addition of CB[7]·**1** with a zoom of a cartoon showing the structure of the [2]rotaxane.

Connecting gold nanoparticles

By utilizing the free thiol functionalities in CB[7]·**2** it was proven possible to build a gold nanoparticle (AuNP) capped [2]rotaxane that is soluble in water. The [2]rotaxane is constructed from a single [2]pseudorotaxane CB[7]·**2** in the centre that is used as an organic linker to connect two AuNP "stoppers" by the self-assembly of the thiols onto the gold surfaces. To show the general nature of the concept, the assembly was carried out using two different sizes of nanoparticles under similar experimental conditions. Notably, a solution of CB[7]·**2** was exposed to either 12 or 60 nm citrate stabilized gold nanoparticles. After the initial reaction, the nanoparticle dimers were purified using centrifugation (see ESI, section S6† for details).

Transmission electron microscopy (TEM) provided structural information on the [2]rotaxane "hybrid" (Fig. 5). The gold nanoparticles appear clearly as solid spheres (12 or 60 nm in diameter) while the [2]pseudorotaxane CB[7]·**2** with a diameter of only ~1.5 nm is too small to see in the images. Without the addition of CB[7]·**2** the gold nanoparticles are dispersed individually. The presence of CB[7]·**2** triggers the formation of AuNP dimers binding two gold nanoparticles together, and forming the desired [2]rotaxane. We note that nanoparticle rotaxane oligomers can be formed during the synthesis, but these higher density structures are removed during centrifugation.[48]

Conclusions

We have described a nanoparticle-stoppered [2]rotaxane based on an exceptionally stable pseudo-rotaxane featuring an electroactive ferrocene rod encapsulated in a cucurbit[7]uril macrocycle. The pure and nano-stoppered rotaxanes have been characterised comprehensively, and the interfacial electrochemical electron transfer patterns have been rationalized by a transparent frame of molecular charge transfer theory. Particularly, we have been able to conclude that the electrochemical electron transfer kinetics proceeds *via* diffusion of **1** and CB[7]·**1** while CB[7]·**2** most likely operates *via* a highly efficient surface controlled mechanism. With these discoveries we have opened new avenues to prepare and manipulate nano-sized objects and systems, where a single or a few isolated active molecules constitute the active units. With the enormous progress in the preparation of molecular machines witnessed in the past few decades, we believe that this work can pave the way to an entirely new type of nano-sized molecular machine.

Conflicts of interest

There are no conflicts to declare.

Acknowledgements

This work was supported by the Lundbeck Foundation and the Danish Council for Independent Research (Sapere Aude, DFF 4148-002606) (M. P.), the Lundbeck Foundation (R141-2013-13273) (J. Z.), and the European Research Council (ERC-StG (G. A. 337221 SIMONE)) (L. S. and K. M.-P.) We thank Christian G. Tortzen for assistance with the ^{1}H–^{1}H ROESY and ^{1}H DOSY NMR experiments.

Notes and references

1 J. F. Stoddart, *Angew. Chem., Int. Ed.*, 2017, **56**, 11094–11125.
2 T. R. Kelly, H. De Silva and R. A. Silva, *Nature*, 1999, **401**, 150–152.
3 N. Koumura, R. W. J. Zijlstra, R. A. van Delden, N. Harada and B. L. Feringa, *Nature*, 1999, **401**, 152–155.
4 C.-F. Lee, D. A. Leigh, R. G. Pritchard, D. Schultz, S. J. Teat, G. A. Timco and R. E. P. Winpenny, *Nature*, 2009, **458**, 314–318.
5 S. D. P. Fielden, D. A. Leigh and S. L. Woltering, *Angew. Chem., Int. Ed.*, 2017, **56**, 11166–11194.
6 N. C. H. Lim and S. E. Jackson, *J. Phys.: Condens. Matter*, 2015, **27**, 354101.
7 J. D. Hegemann, M. Zimmermann, X. Xie and M. A. Marahiel, *Acc. Chem. Res.*, 2015, **48**, 1909–1919.
8 S. S. Jang, Y. H. Jang, Y.-H. Kim, W. A. Goddard, A. H. Flood, B. W. Laursen, H.-R. Tseng, J. F. Stoddart, J. O. Jeppesen, J. W. Choi, D. W. Steuerman, E. DeIonno and J. R. Heath, *J. Am. Chem. Soc.*, 2005, **127**, 1563–1575.
9 Q. Zhang, W.-Z. Wang, J.-J. Yu, D.-H. Qu and H. Tian, *Adv. Mater.*, 2017, **29**, 1604948.
10 Q. Zhang and D.-H. Qu, *ChemPhysChem*, 2016, **17**, 1759–1768.
11 A. K. Boal and V. M. Rotello, *J. Am. Chem. Soc.*, 2000, **122**, 734–735.

12 P. Nowak, V. Saggiomo, F. Salehian, M. Colomb-Delsuc, Y. Han and S. Otto, *Angew. Chem., Int. Ed.*, 2015, **54**, 4192–4197.
13 A. Cecconello, C.-H. Lu, J. Elbaz and I. Willner, *Nano Lett.*, 2013, **13**, 6275–6280.
14 M.-C. Daniel and D. Astruc, *Chem. Rev.*, 2004, **104**, 293–346.
15 E. Katz and I. Willner, *Angew. Chem., Int. Ed.*, 2004, **43**, 6042–6108.
16 A. M. Alkilany, S. E. Lohse and C. J. Murphy, *Acc. Chem. Res.*, 2013, **46**, 650–661.
17 M. R. Dewi, T. A. Gschneidtner, S. Elmas, M. Ranford, K. Moth-Poulsen and T. Nann, *ACS Nano*, 2015, **9**, 1434–1439.
18 L. Sun, Y. A. Diaz-Fernandez, T. A. Gschneidtner, F. Westerlund, S. Lara-Avila and K. Moth-Poulsen, *Chem. Soc. Rev.*, 2014, **43**, 7378–7411.
19 Y. D. Fernandez, L. Sun, T. Gschneidtner and K. Moth-Poulsen, *APL Mater.*, 2014, **2**, 010702.
20 T. A. Gschneidtner, Y. A. D. Fernandez and K. Moth-Poulsen, *J. Mater. Chem. C*, 2013, **1**, 7127–7133.
21 A. Guttman, D. Mahalu, J. Sperling, E. Cohen-Hoshen and I. Bar-Joseph, *Appl. Phys. Lett.*, 2011, **99**, 063113.
22 A. B. Petersen, E. Thyrhaug, T. Jain, K. Kilsaa, M. Bols, K. Moth-Poulsen, N. Harrit and T. Bjørnholm, *J. Phys. Chem. B*, 2010, **114**, 11771–11777.
23 S. Karmakar, S. Kumar, P. Marzo, E. Primiceri, R. Di Corato, R. Rinaldi, P. G. Cozzi, A. P. Bramanti and G. Maruccio, *Nanoscale*, 2012, **4**, 2311–2316.
24 M. V. Rekharsky, T. Mori, C. Yang, Y. H. Ko, N. Selvapalam, H. Kim, D. Sobransingh, A. E. Kaifer, S. Liu, L. Isaacs, W. Chen, S. Moghaddam, M. K. Gilson, K. Kim and Y. Inoue, *Proc. Natl. Acad. Sci. U. S. A.*, 2007, **104**, 20737–20742.
25 G. C. Lloyd-Jones, J. D. Moseley and J. S. Renny, *Synthesis*, 2008, 661–689.
26 C. Glidewell, B. J. L. Royles and D. M. Smith, *J. Organomet. Chem.*, 1997, **527**, 259–261.
27 C. Marquez, H. Fang and W. M. Nau, *IEEE Trans. Nanobioscience*, 2004, **3**, 39–45.
28 W. S. Jeon, K. Moon, S. H. Park, H. Chun, Y. H. Ko, J. Y. Lee, E. S. Lee, S. Samal, N. Selvapalam, M. V. Rekharsky, V. Sindelar, D. Sobransingh, Y. Inoue, A. E. Kaifer and K. Kim, *J. Am. Chem. Soc.*, 2005, **127**, 12984–12989.
29 L. Cao, M. Šekutor, P. Y. Zavalij, K. Mlinarić-Majerski, R. Glaser and L. Isaacs, *Angew. Chem., Int. Ed.*, 2014, **53**, 988–993.
30 C. A. Schalley, *Analytical Methods in Supramolecular Chemistry*, Wiley, 2007.
31 N. M. Green, *Biochem. J.*, 1963, **89**, 585–591.
32 D. Bardelang, K. A. Udachin, D. M. Leek, J. C. Margeson, G. Chan, C. I. Ratcliffe and J. A. Ripmeester, *Cryst. Growth Des.*, 2011, **11**, 5598–5614.
33 S. Mecozzi and J. J. Rebek, *Chem. – Eur. J.*, 1998, **4**, 1016–1022.
34 F. Yang and D. V. Dearden, *Isr. J. Chem.*, 2011, **51**, 551–558.
35 S. Yi, W. Li, D. Nieto, I. Cuadrado and A. E. Kaifer, *Org. Biomol. Chem.*, 2013, **11**, 287–293.
36 N. G. Connelly and W. E. Geiger, *Chem. Rev.*, 1996, **96**, 877–910.
37 W. Ong and A. E. Kaifer, *Organometallics*, 2003, **22**, 4181–4183.
38 L. Cui, S. Gadde, W. Li and A. E. Kaifer, *Langmuir*, 2009, **25**, 13763–13769.
39 S. Senler, W. Li, M. H. Tootoonchi, S. Yi and A. E. Kaifer, *Supramol. Chem.*, 2014, **26**, 677–683.
40 R. C. Engstrom and V. A. Strasser, *Anal. Chem.*, 1984, **56**, 136–141.
41 J. E. B. Randles, *Trans. Faraday Soc.*, 1948, **44**, 327–338.
42 A. J. Bard and L. R. Faulkner, *Electrochemical Methods: Fundamentals and Applications*, Wiley, 2nd edn, 2001.
43 S. Gadde and A. E. Kaifer, *Curr. Org. Chem.*, 2011, **15**, 27–38.
44 D. K. Gosser, *Cyclic Voltammetry: Simulation and Analysis of Reaction Mechanisms*, Wiley, 1993.
45 R. S. Nicholson, *Anal. Chem.*, 1965, **37**, 1351–1355.
46 A. M. Kuznetsov and J. Ulstrup, *Electron transfer in chemistry and biology - An introduction to the theory*, Wiley, 1998.
47 E. Laviron, *J. Electroanal. Chem.*, 1979, **101**, 19–28.
48 F. C.-M. Leung, S. Y.-L. Leung, C. Y.-S. Chung and V. W.-W. Yam, *J. Am. Chem. Soc.*, 2016, **138**, 2989–2992.

